Heat transfer enhancement by recirculating flow within liquid plugs in microchannels

ZhizhaoChe, TeckNeng Wong*, Nam-Trung Nguyen

School of Mechanical and Aerospace Engineering, Nanyang Technological University, 50 Nanyang Avenue, Singapore 639798, Singapore

**Corresponding Author. Tel.: +65 67905587; fax: +65 67911859*
E-mail address: mtnwong@ntu.edu.sg (T.N. Wong).

Abstract:

Plug flow can significantly enhance heat transfer in microchannels as compared to single phase flow. Using an analytical model of flow field, heat transfer in plug flow is investigated. The constant-surfacetemperature boundary condition is considered. Three stages of the heat transfer in plugs are identified: (i) development of thermal boundary layer; (ii) advection of heated/fresh fluid in the plug; and (iii) thermally fully developed flow. Due to the transport of heated fluid and fresh fluid within the plug by the recirculating flow, oscillations of the Nusselt number at high Peclet numbers are observed and explained. The effects of the Peclet number and the plug length on the heat transfer process are evaluated. The results show that short plugs are preferable to long plugs since short plugs result in high Nusselt numbers and high heat transfer indices.

1. Introduction

The miniaturization of electronic devices leads to denser packaging of components. Micro heat exchangers are required to cope with the high heat flux produced in the microdevices. Microchannel heat exchangers [1,2] are possible with the development of various microfabrication techniques, while the advances in micro-fluidics [3] deepen our understanding of the heat transfer phenomena in microchannels.

Microchannel heat exchangers have the advantages of large contact area and large temperature gradient between the wall and the fluids. However, flow in microchannels is usually laminar with low Reynolds numbers [3]. Extremely high pressure is required to produce turbulence in microchannels. Without turbulence to disturb the flow, heat transfer in microchannels is limited by the thermal diffusion process.

Scalars can be transported or mixed in fluids with the help of vortices. With a

recirculating flow, heat or mass can be advected by the flow even in the Stokes regime, during which the Reynolds number is so small that the inertial force is negligible [4]. Liquid filaments can be continuously stretched and folded by recirculating flow, and interfacial area between liquid filaments can be greatly increased. If vortices are of sufficient size and strength, their enhancement of heat or mass transfer can be significant [5].

Many methods to enhance heat transfer reported in the literature can be categorized into the group of promoting vortices. For example, curved channels have been used to produce Dean vortices [6] to enhance heat transfer [7–9]. The Dean vortices are a type of secondary flow consisting of a pair of counter rotating vortices resulted from the imbalance between the centrifugal force and the radial pressure difference when the fluid passes through a curved channel. The vortices get stronger when the Dean number increases, which characterizes the relative effect of force with the viscous force, $De = \frac{\rho V D_H}{\mu}\sqrt{\frac{D_H}{2R}}$,where ρ and μ are centrifugal respectively the density and the dynamic viscosity of the fluid, V is the axial velocity, D_H is the hydraulic diameter of the channel, and R is the radius of the curved channel path. In microchannels, however, due to the low velocity, the centrifugal force and the Dean number are small. Consequently, the Dean vortices are much weaker than that in channels of large scale.

Another way to promote vortices in microchannels is to use vortex promoters [10], which are usually one or arrays of built-in obstacles in microchannels. Vortex promoters of different shapes (such as square [11], rectangular [12], triangular [13], and circular [10,14]) can produce transverse flow by flow separation on the surface of the vortex promoters, which results from the interplay between the inertial force and the viscous force. The vortex strength increases with increasing the Reynolds number ($Re = \rho VD_H/\mu$), which enhances the heat transfer process. In microchannels, however, the transfer of momentum, mass, and energy takes place in the laminar regime and is characterized by low Reynolds numbers [3], which restricts the application of vortex promoters to enhance heat transfer. Moreover, the cost to fabricate the obstacles in microchannels is much higher than that to fabricate simple smooth channels.

A simple and effective method to induce vortices in microchannels is by introducing interfaces into the flow. When a second immiscible fluid is introduced into a microchannel, interfaces of different shapes are formed which correspond to different flow patterns, such as bubble/droplet flow, plug flow, annular flow, and stratified flow [15,16]. Plug flow, also called slug flow, segmented flow, Taylor flow, is a flow structure where the liquid adopts a plug shape and occupies the entire width of the micro-channel [17]. Plug flow can be formed by continuously generating droplets/bubbles in microchannels [18]. As the size dispersity of the droplets/bubbles can be as low as 2%, this ordered structure makes it possible to manipulate the flow and transportation in droplets/plugs accurately. In the presence of the interface,

vortices are formed in liquid plugs [19,20]. Unlike vortex promoters, in which vortices are formed locally in the region behind the obstacles, vortices produced by plug flow occupy the whole plug. Therefore, it possesses the advantage that the vortices in plugs can be used to enhance heat and mass transfer in microchannels. Existing investigations have shown that mixing of species in plugs can be significantly enhanced [21–25].

Plug flow shows promising opportunities in heat exchangers by inducing vortices [26], and the flow can be induced by pressure using pumps [27] or electrowetting on dielectric (EWOD) [26,28] method. However, systematic investigations of heat transfer enhancement in plugs are few, and heat transfer in two phase flow in microchannels has not been studied as extensively as single phase flow [2]. A possible reason is that two phase flow is much more complex than single phase flow. Some previous work dealing with heat transfer of multiphase flow in microchannels mainly contributed to boiling [29,30] and condensation [31]. The effects of phase change on the Nusselt number or convective heat transfer coefficient were investigated, while the effects of the vortices on heat transfer were not quantified.

To experimentally investigate the effect of the vortices in droplets/plugs on the heat transfer process, it is necessary to characterize the interaction between the velocity field and the temperature field. Micro particle imaging velocimetry (μPIV) is a tool widely used to assess the flow field in microchannels; while laser induced fluorescence (LIF) method is a technique to measure the temperature field in microchannels. Both methods require the refractive indices of different phases to match to ensure the optical access without distortion at fluid interfaces [32,33]. Moreover, most materials used for heat exchangers are not transparent to visible light, which increases difficulties in using these optical methods (μPIV and LIF). In the experimental investigations of heat transfer in a stainless steel tube (1.5 mm internal bore) done by Walsh et al. [27], the surface temperature on the stainless tube was obtained using a high resolution infrared thermography system, but the temperature field in the liquid plug could not be measured. During the heat transfer process, the temperature of the plug is usually neither uniform nor identical to the wall temperature.

To numerically and analytically model the heat transfer process of plug flow in microchannels, both the flow field and the temperature field should be considered. Muzychka et al. [34] proposed a simplified model to consider the heat transfer in plugs in micro-channels of different cross-sectional shapes. The heat transfer process was considered as a Graetz problem with a steady state condition. The problem was solved analytically by assuming a uniform velocity profile throughout the liquid plug. A better way is to incorporate the recirculating flow in the liquid plug into the model of heat transfer and to investigate how the recirculating vortices affect the heat transfer process.

To numerically simulate the heat transfer process of plug flow in microchannels,

numerical methods to predict the location and the shape of the interface are often necessary. This type of numerical methods to predict the interface includes the front tracking method [22], the volume of fluid method [35,36], the level set method [37,38], the Lattice Boltzmann method [39,40], and the moving-grid method [41]. These approaches are usually complex and computation-time consuming, which are unfavourable for heat transfer analysis in plug flow in microchannels.

In order to understand the heat transfer process of plug flow in microchannels, here we solve the energy equation within plug flow based on the analytical two-dimensional flow field [42]. Without numerically solving the flow field, it is a simple and efficient way to analyze the influence of the recirculating vortices on the heat transfer process in plugs. This paper is organized as follows. The mathematical formulas are provided in Section 2, including the analytical flow field in the liquid plug and the numerical method for the heat transfer process. In Section 3, the stages of heat transfer are identified, and compared with single phase flow. The effects of different Peclet numbers and different plug lengths are analyzed and explained.

2. Mathematical modelling

2.1. Modelling of flow field in liquid plugs

To model a liquid plug in a 2D microchannel, the following dimensionless quantities are introduced,

$$\hat{x} \equiv x/w, \quad \hat{y} \equiv y/w, \quad \hat{u}_x \equiv u_x/V, \quad \hat{u}_y \equiv u_y/V, \quad \widehat{L} \equiv L/w \tag{1}$$

where w is the width of the microchannel, V is the speed of the liquid plug, and L is the length of the liquid plug. The dimensionless form of the velocity field in the liquid plug [42] is

$$\begin{aligned}\hat{u}_x = \sum_{n=1,3,5,\ldots}^{\infty} & \sin(\beta_n \hat{x})[C_{2n}\beta_n \cosh(\beta_n \hat{y}) + C_{3n}\beta_n \hat{y} \sinh(\beta_n \hat{y}) \\ & + C_{3n} \cosh(\beta_n \hat{y}) + C_{4n}\beta_n \hat{y} \cosh(\beta_n \hat{y}) + C_{4n} \sinh(\beta_n \hat{y})]\end{aligned} \tag{2}$$

$$\begin{aligned}\hat{u}_y = - \sum_{n=1,3,5,\ldots}^{\infty} & \beta_n \cos(\beta_n \hat{x}) \\ & \times [C_{2n} \sinh(\beta_n \hat{y}) + C_{3n}\hat{y} \cosh(\beta_n \hat{y}) + C_{4n}\hat{y} \sinh(\beta_n \hat{y})]\end{aligned} \tag{3}$$

where

$$C_{2n} = -\frac{4}{D_n \widehat{L} \beta_n} \sinh(\beta_n) - \frac{4}{D_n \widehat{L}} \tag{4}$$

$$C_{3n} = \frac{4}{D_n \widehat{L}} \sinh(\beta_n) + \frac{4\sinh^2(\beta_n)}{\widehat{L}\beta_n D_n} \tag{5}$$

$$C_{4n} = \frac{4}{D_n \widehat{L}\beta_n} [-\beta_n \cosh(\beta_n) + \sinh(\beta_n) - \sinh(\beta_n)\cosh(\beta_n) + \beta_n] \tag{6}$$

$$D_n = \beta_n^2 - \sinh^2(\beta_n) \tag{7}$$

$$\beta_n = n\pi/\widehat{L} \tag{8}$$

2.2. Analysis of heat transfer

To analyze the heat transfer in a liquid plug, we consider the energy conservation of the plug with a translating frame of reference following the plug. For an incompressible Newtonian fluid with constant properties and without source term, the energy conservation equations is

$$\frac{\partial(T)}{\partial t} + \frac{\partial(u_x T)}{\partial x} + \frac{\partial(u_y T)}{\partial y} = \frac{k}{\rho c_p}\left(\frac{\partial^2 T}{\partial x^2} + \frac{\partial^2 T}{\partial y^2}\right) \tag{9}$$

where$T$ is the temperature, ρ is the density of the fluid, k is the thermal conductivity, and c_p is the specific heat capacity. We introduce the following dimensionless variables,

$$\hat{t} \equiv \frac{t}{\tau}, \quad Pe \equiv \frac{wV}{\alpha}, \quad \widehat{T} \equiv \frac{T - T_0}{T_w - T_0} \tag{10}$$

where $\tau \equiv w/V, \alpha \equiv \frac{k}{\rho c_p}$,$T_0$ is the inlet temperature, and T_w is the wall temperature. The dimensionless form of the energy equation is obtained as follows,

$$\frac{\partial(\widehat{T})}{\partial \hat{t}} + \frac{\partial(\hat{u}_x \widehat{T})}{\partial \hat{x}} + \frac{\partial(\hat{u}_y \widehat{T})}{\partial \hat{y}} = \frac{1}{Pe}\left(\frac{\partial^2 \widehat{T}}{\partial \hat{x}^2} + \frac{\partial^2 \widehat{T}}{\partial \hat{y}^2}\right) \tag{11}$$

where$Pe \equiv wV/\alpha$ is the Peclet number which characterizes the ratio of the rate of heat advection caused by the flow to the rate of heat diffusion driven by the temperature gradient. With this normalization, the dimensionless time$\hat{t}$ and the dimensionless axial location of the plug in the microchannel$\widehat{X}$ is related as

$$\hat{t} = \widehat{X} \tag{12}$$

The flow field, as it is directly known from the analytical solution in Eqs. (2) and (3), is substituted into Eq. (11) for the heat transfer analysis. Eq. (11) was discretized using the finite volume method (FVM) on staggered grids [43].

Before entering the microchannel, the liquid plug has an initial uniform temperature field with $\hat{T}= 0$. When moving in the micro-channel, the plug is subjected to a constant-surface-temperature boundary condition on the wall of the microchannel, as shown in Fig. 1.

With constant surface temperature T_w maintained on the wall of the microchannel, the boundary condition is

$$T = T_w \quad \text{at} \quad y = 0 \quad \text{or} \quad y = w \tag{13}$$

and in dimensionless form,

$$\hat{T} = 1 \quad \text{at} \quad \hat{y} = 0 \quad \text{or} \quad \hat{y} = 1 \tag{14}$$

2.3. Evaluation of heat transfer

To characterize the heat transfer capabilities of plug flow along the microchannel, and to compare with the continuous single phase flow, we use two quantities, namely Nusselt number *Nu* (Section 2.3.1) and heat transfer index η (Section 2.3.2). To compare between the single phase flow and the plug flow, these two quantities are calculated (i) at a specific axial location $\hat{X}$ for the single phase flow, as illustrated in Fig. 2a; and (ii) for the plug flow at the instant when the plug passes the same axial location, i.e., $\hat{t}=\hat{X}$, as illustrated in Fig. 2b.

2.3.1. Nusselt number

To evaluate the convective heat transfer, the Nusselt number is defined as the ratio of convective to conductive heat transfer normal to the wall,

$$Nu \equiv \frac{hD_H}{k} \tag{15}$$

where the hydrodynamic diameter of the channel is $D_H= 2w$. To analyze the convective heat transfer coefficient of the plug flow h, the mean fluid temperature of a plug unit $\overline{T}_{\text{plug}}$ is used as the reference temperature [44], which refers to the mean fluid temperature of the plug at the axial location *X*, and is defined as

$$\overline{T}_{\text{plug}}(X) \equiv \frac{\int_{A_{\text{plug}}} \rho c_p u_x T dA_{\text{plug}}}{\int_{A_{\text{plug}}} \rho c_p u_x dA_{\text{plug}}} \tag{16}$$

Therefore, in dimensionless form, the mean fluid temperature of the plug is

$$\widehat{\overline{T}}_{\text{plug}}(\widehat{X}) \equiv \frac{\int_0^1 d\hat{y} \int_0^{\widehat{L}} \hat{u}_x \widehat{T} d\hat{x}}{\int_0^1 d\hat{y} \int_0^{\widehat{L}} \hat{u}_x d\hat{x}} \tag{17}$$

Similarly, for the single phase flow, the mean fluid temperature $\widehat{\overline{T}}_{sp}(\widehat{X})$ refers to the mean temperature of the fluid over the cross section $\widehat{X}$ of the channel, and in dimensionless form, it is [44]

$$\widehat{\overline{T}}_{\text{sp}}(\widehat{X}) \equiv \frac{\int_0^1 \hat{u}_x \widehat{T} d\hat{y}}{\int_0^1 \hat{u}_x d\hat{y}} \tag{18}$$

2.3.1.1. Nusselt number for single phase flow. For the continuous single phase flow in microchannels, the convective heat transfer coefficient is

$$h_{\text{sp}} \equiv \frac{-k(\partial T/\partial y)_{y=0}}{T_{\text{w}} - \overline{T}} \tag{19}$$

where the subscript 'sp' refers to the single phase flow. By substituting Eqs.(18) and (19) into Eq.(15), the Nusselt number can be expressed by dimensionless variable as follows,

$$Nu_{\text{sp}} = \frac{-2(\partial \widehat{T}/\partial \hat{y})_{\hat{y}=0}}{1 - \widehat{\overline{T}}} \tag{20}$$

2.3.1.2. Nusselt number for plug flow. For plug flow in microchannels, the convective heat transfer coefficient h for a plug unit can be calculated as a function of the axial location ($\widehat{X}$) as the temperature inside the plug develops. It is calculated based on the average heat flux, the average temperature difference, and the mean fluid temperature of the plug unit. In the constant-surface-temperature condition, we have

$$h_{\text{plug}} \equiv \frac{\int_0^L (-k\partial T/\partial y)_{y=0} dx}{\int_0^L (T_w - \overline{T}) dx} \tag{21}$$

where the subscript 'plug' refers to the plug flow. The Nusselt number, expressed by dimensionless variables, is

$$Nu_{\text{plug}} = \frac{2\int_0^{\hat{L}} (-\partial \hat{T}/\partial \hat{y})_{\hat{y}=0} d\hat{x}}{\int_0^{\hat{L}} (1 - \widehat{\overline{T}}) d\hat{x}} \tag{22}$$

2.3.2. Heat transfer index

Heat transfer index, $\eta(\hat{X}) \equiv Q(\hat{t})/Q_{\max}$, is defined as a function of the axial location $\hat{X}$ to characterize the progress of the heat transfer in the microchannel, where $Q_{\max}$ is the maximum amount of energy transfer that could occur if the process continues to $\hat{t} \to \infty$, while $Q(\hat{t})$ is the total energy transferred from the wall to the plug over the time interval 0 to $\hat{t}$. With a constant surface temperature maintained on the wall, the maximum possible energy $Q_{\max}$ corresponds to the condition when the whole plug unit has achieved the uniform wall temperature. Therefore, assuming constant fluid properties, the heat transfer index is

$$\eta_{\text{plug}}(\hat{X}) \equiv \frac{Q(\hat{t})}{Q_{\max}} = \frac{\int_0^w dy \int_0^L \rho c_p (T - T_0) dx}{\int_0^w dy \int_0^L \rho c_p (T_w - T_0) dx} = \frac{1}{\hat{L}} \int_0^1 d\hat{y} \int_0^{\hat{L}} \hat{T} d\hat{x} \tag{23}$$

The heat transfer index varies from 0 to unity as heat transfer progresses. η = 0 implies that heat transfer has not begun yet, while η= 1 implies that the plug unit has achieved the wall temperature. The variation of the heat transfer index against the axial location $\hat{X}$ indicates the progress of heat transfer in the microchannel.

For single phase flow, a corresponding heat transfer index is defined to evaluate the progress of the heat transfer at the cross section $\hat{X}$of the microchannel as follows,

$$\eta_{\text{sp}}(\hat{X}) \equiv \frac{Q(\hat{X})}{Q_{\max}} = \frac{\int_0^w \rho c_p (T - T_0) dy}{\int_0^w \rho c_p (T_w - T_0) dy} = \int_0^1 \hat{T} d\hat{y} \tag{24}$$

3. Results and discussion

3.1. Flow field in a typical liquid plug

The flow field in a typical liquid plug, as shown in Fig. 3, is dominated by two symmetrical vortices as the plug moves forward (from left to right). When the liquid in the plug moves towards the front of the plug, it is blocked by the front interface, changing the flow direction towards the wall of the microchannel. At the wall of the microchannel, due to the friction of the wall, the liquid moves backward with respect to the translating frame of reference. At the rear of the liquid plug, due to the presence of the rear interface, liquid moves from the wall of the microchannel towards the centre of the plug. Consequently, the presence of the front/rear interfaces produces a

recirculating flow pattern in the liquid plug. The transverse flow of the recirculating vortices in the plug is crucial to enhance heat transfer between the wall and the liquid, and it will be explained in Sections 3.2 and 3.4.

3.2. Heat transfer process and comparison with single phase flow

The time evolution of the isotherms for a liquid plug moving through a 2D microchannel is shown in Fig. 4a (Instants A–H), and their corresponding points are marked in Fig. 4b. The channel wall is subjected to a constant temperature $\hat{T}_w$ = 1, the dimensionless plug length is $\hat{L}$= 2, and the Peclet number is *Pe* = 100. The variation of the Nusselt number *Nu*, the wall temperature $\hat{T}_w$ = 1, and the mean fluid temperature of the plug b $\hat{\bar{T}}_{\text{plug}}$ [Eq. (17)] are plotted against time in Fig. 4b. To compare between the plug flow and the single phase flow, the Nusselt number *Nu* and the heat transfer index η are plotted in Fig. 4c and d, respectively.

For the single phase flow, we assume that the flow is fully developed hydrodynamically but thermally developing. The Nusselt number is large near the entrance and decays along the channel to an asymptotic limit ($Nu_{\text{asymp,sp}}$= 7.5) due to the development of the thermal boundary layer along the wall, while the heat transfer can be divided into the thermal entrance region and the fully developed region according to the thickness of the thermal boundary layer, as shown in Fig. 4c.

In contrast, for the plug flow, heat transfer is initiated when the plug enters the microchannel, followed by three subsequent stages of convective heat transfer between the plug and the heated wall: (i) development of thermal boundary layer; (ii) advection of heated/fresh fluid in the plug; and (iii) thermally fully developed flow.

Stage I: *Development of thermal boundary layer* (TBL), (Fig. 4a and b (Instants B–C)): At the instant that the plug contacts the heated wall, a large temperature difference is formed between the plug and the wall since the plug temperature is uniformly distributed ($\hat{T}$= 0) while the wall temperature is maintained at $\hat{T}_{\text{w}}$ =1.The thin liquid layer in the immediate vicinity of the wall rapidly achieves thermal equilibrium with the wall and forms a thermal boundary layer, (Fig. 4a (Instant B)). The effect of the wall temperature on the fluid outside the TBL is negligible. In the translating frame of reference following the plug, the fluid velocity in the region near the channel wall is negative as shown in Fig. 3, and the fluid particles in the TBL moves from the front interface to the rear interface. Hence, the TBL is thinner near the front interface, while it is thicker near the rear interface. As time passes, the effects of heat transfer penetrate further into the plug and the thickness of the TBL grows, until the TBL reaches the centreline of the channel (Fig. 4a (Instant C)), which marks the end of Stage I and the beginning of Stage II.

The TBL is extremely thin when it is initially formed, resulting in a large *Nu*. With the development of the TBL with time, Nu decreases dramatically.

TBLs in plug flow have two distinctive features as compared with single phase flow. (i) The thickness of the TBL for plug flow is not only a function of space, but also a function of time. (ii) In single phase flow, fluids usually approaches the wall along the wall direction, while in plug flow, fluids in the plug approaches the wall in the perpendicular direction due to the presence of the front interface. Similarly, at the rear interface, fluids leave the wall in the perpendicular direction due to the presence of the rear interface. Therefore, TBLs in plug flow are more complex than those in single phase flow.

Stage II: *Advection of heated/fresh fluid in the plug*, (Fig. 4a and b (Instant D–F)): At the rear of the plug, due to the presence of the rear interface, the heated fluid moves towards the central region of the plug. And in the central region, the fluid temperature decreases as the fluid travels in the plug moving direction (Fig. 4a (Instant E)) due to: (i) less influence from the heated channel wall and (ii) thermal mixing with the fresh fluid originally in the central region. At the same time, due to the presence of the front interface, the fresh fluid from the central region of the plugmoves transversely to the heated channel wall. In this manner, the heated and the fresh fluids are advected within the plug by the recirculating vortices. As time progresses, the temperature difference between the heated fluid and the fresh fluid decreases, until there is no distinct interface between the heated fluid and the fresh fluid, which marks the end of Stage II and the beginning of Stage III.

At Stage II, the advection of the heated/fresh fluid results in the variation of the heat flux on the wall and the oscillation of the Nusselt number, as shown in Fig. 4b. The details will be discussed in Section 3.3.

Stage III: *Thermally fully developed flow*, (Fig. 4a and b (Instants G to H)): This stage is characterized by the shapes of the temperature contours within the liquid plug. Although the absolute value of the fluid temperature gradually approaches T_w, the shapes of the temperature contours remain unchanged over time (Fig. 4a (Instant G to H)). With the unchanged temperature pattern, the Nusselt number approaches an asymptotic limit, $Nu_{\text{asymp,plug}}$ = 31.3, which is much higher as compared with single phase flow ($Nu_{\text{asymp,sp}}$= 7.5), as shown in Fig. 4c. If the channel is sufficiently long, heat transfer continues until the fluid temperature reaches a uniform temperature being the same as the wall.

In fully developed single phase flow, the streamlines are straight along the channel path. Heat transfer in the transverse direction is via conduction. Only the fluid flowing near the channel wall is being heated while the fluid near the central region of the channel remains slightly higher than the inlet temperature.

Plug flow, however, creates internal recirculating flow due to high shearing interactions with the channel wall and the presence of the front/rear interfaces. The recirculating flow induces a substantial amount of transverse thermal mixing in the fluid. This transverse convection brings heated liquid from the channel wall to the

central region at the rear interface, allows thermal mixing of fluids within the plug, and subsequently transports it back to the wall. In addition, the liquid filament in the plug is stretchedby the recirculating flow, which causes an effect of Taylor dispersion [45] among liquid filaments. Although Taylor dispersion exists in single phase flow, the Taylor dispersion of heat in plugs between liquid filaments is confined within spaces of nanolitre scale. Therefore, the Taylor dispersion within the liquid plug is stronger and more effective to enhance heat transfer.

Fig. 4d compares the heat transfer index η between plug flow and single phase flow. It can be seen that to achieve a given heat transfer index, the required channel length will be significantly shorter to use plug flow than to use single phase flow. These results indicate the heat transfer enhancement by the plug flow.

3.3. Effect of Peclet number

The effect of the Peclet number on the Nusselt number and the heat transfer index is shown in Fig. 5a and b, respectively. In the simulation, the dimensionless plug length is fixed at $\hat{L}$= 2 and *Pe* is varied from 4 to 1024. Fig. 5a shows that the Nusselt number increases with increasing the Peclet number. At a low Peclet number (*Pe* = 4), the Nusselt number achieves a lower asymptotic limit ($Nu_{\text{asymp},Pe=4}$ = 8.5) at Stage III, while at a high Peclet number (*Pe* = 1024), the transport process is dominated by advection, and the asymptotic limit of the Nusselt number at Stage III is higher ($Nu_{\text{asymp},Pe=1024}$= 42.4). The influence of the Peclet number on the heat transfer index shows that the heat transfer index decreases with increasing *Pe*. This is because a fast flow (a high Peclet number) results in a short residence time in the heated channel.

The Nusselt number for a plug unit, especially at large Peclet numbers, exhibits an oscillatory behaviour, as shown in Fig. 5a. To analyze the oscillation of *Nu*, *Nu* at a high Peclet number (*Pe* = 1024) is plotted in Fig. 6a, as well as the two important factors that influence *Nu*, namely the mean value of temperaturegradient at the wall over the plug length $\left[\overline{-\partial\hat{T}/\partial\hat{y}} \equiv \frac{1}{\hat{L}}\int_0^{\hat{L}}(-\partial\hat{T}/\partial\hat{y})_{\hat{y}=0}d\hat{x}\right]$, and the mean fluid temperature of the plug unit [$\hat{\bar{T}}_{\text{plug}}$ in Eq. (17)]. The temperature distribution in the plug at some typical instants are shown in Fig. 6b. From the variation of $\overline{-\partial\hat{T}/\partial\hat{y}}$, and the temperature field, we can see that the oscillation of *Nu* is caused by the recirculating flow in the plug. When the fresh fluid in the central region of the plug is being transported to the heated wall by the recirculating flow (Fig. 6 Instants A–D), $\overline{-\partial\hat{T}/\partial\hat{y}}$, is large due to the high temperature difference betweenthe wall and the liquid. In addition, $\overline{-\partial\hat{T}/\partial\hat{y}}$, remains constant during this period because fresh fluid is continuously transported to the heated wall by the recirculating flow. In the meantime, themean fluid temperature of the plug unit $\hat{\bar{T}}_{\text{plug}}$ increases smoothly as shown in Fig. 6a. Hence, according to Eq. (22), *Nu* increases in this period. As the heated fluid in the

plug is transported back tothe heated wall (Fig. 6b (Instants D–F)), $\overline{-\partial\hat{T}/\partial\hat{y}}$, immediately decreases, which results in a decrease in the heat flux and a decrease in *Nu* (Fig. 6a (Instants D–F)). This oscillation of *Nu* is damped asthe temperature difference between the fresh fluid and the heated fluid reduces until there is no distinct interface between the fresh fluid and the heated fluid.

To quantitatively compare the heat transfer between single phase flow and plug flow at different Peclet numbers, the heat transfer indices at the axial location of the channel $\hat{X}$= 10 are calculated and plotted against Peclet number in Fig. 7. The temperature distributions in the plug at different Peclet numbers are also shown. At a small Peclet number (*Pe* = 4), the heat transfer index is 1 for both single phase flow and plug flow. This means that the fluid has achieved the uniform temperature being the same as the wall. At a large Peclet number (such as *Pe* = 1024), the heat transfer indices are quite different between plug flow and single phase flow. From single phase flow to plug flow, the heat transfer index increases from 0.26 to 0.44. If considering the fact that the growth rate of the heat transfer index ($d\eta/d\hat{X}$) decreases almost exponentially as the fluid flows to the downstream (Fig. 5b), we can conclude that the plug flow can significantly reduce the requirement of the channel length and enhance the heat transfer.

3.4. Effect of plug length

Flow fields in plugs are important to the heat transfer process. In order to study the influence of plug length on heat transfer, its effects on the flow field are analyzed first in this section.

3.4.1. Effect of plug length on transverse velocity and recirculating period

The heat transfer in plugs is enhanced by the recirculating flow, or more specifically, by the transverse flow near the front and the rear interfaces. Therefore, the magnitude of the transverse velocity is an important factor influencing the heat transfer. The transverse velocity at a typical cross section inside the plug ($\hat{y}$ = 3/4) is plotted in Fig. 8 for different plug lengths. The velocity fields of the respective plug length are also shown in Fig. 8. For long plugs ($\hat{L}$ = 4), the transverse component is almost zero at most axial distance of the plug ($0.2 \leq \hat{x}/\hat{L} \leq 0.8$) except in regions close to the front/rear interfaces. In contrast, for short plugs ($\hat{L}$ = 1), the transverse component is significant. Therefore, the recirculating flow in short plugs is more effective in transporting fresh fluid from thecentral region of the plug to the wall and the heated fluid from the wall back to the plug centre.

Another significant factor influencing the heat transfer is the recirculating period $\hat{t}_{\text{recirc}}$, which refers to the time interval for a fluid particle in the plug travelling for one

cycle and getting back to its starting point. The fluid particles follow their streamlines when they are advected by the flow. Therefore, $\hat{t}_{\text{recirc}}$ does not only represent the recirculating period for one particle, but for all the fluid particles along the streamline. In Fig. 9, a column of passive tracer particles (along the middle cross section $\hat{x} = \hat{L}/2$ as shown in the inset of Fig. 9) are tracked using the fourth-order Runge– Kutta (RK) method, and the recirculating periods are calculated for different plug lengths. As the plug length increases, the recirculating period increases significantly. This is because in long plugs, the fluid particles need to travel a long distance along the streamlines. For long plugs ($\hat{L}$= 4), the curve of $\hat{t}_{\text{recirc}}$ versus transverse position $\hat{y}$ has two peaks which correspond to the two vortex centres (or stagnant points) within the plug.

3.4.2. Effect of plug length on heat transfer

The effect of plug length on the Nusselt number is shown in Fig. 10a. In the simulation, the Peclet number is fixed at 100 and the dimensionless plug length is varied from 1 to 4. For short liquid plugs ($\hat{L}$= 1), due to the development of the thermal boundary layer (Stage I), *Nu* decreases and achieves a minimum value of 21.3 at $\hat{X}$ = 0.8. As the plug is moving forward, *Nu* increases and reaches a maximum value of 39 at $\hat{X}$ = 4.2 (Stage II). After that, *Nu* decreases slowly and approaches an asymptotic limit $Nu_{\text{asymp},\hat{L}=1}$ = 34.6 (stage III). The oscillation of the Nusselt number is due to the recirculating flow as discussed in Section 3.3. For long plugs ($\hat{L}$= 4), *Nu* reaches its minimum value of 13.2 at $\hat{X}$= 2.3. The increase in $\hat{X}$ at which point *Nu* reaches its minimum value is because the recirculating period $\hat{t}_{\text{recirc}}$ increases with increasing $\hat{L}$ (Fig. 9). The Nusselt number for $\hat{L}$ =4 finally attains an asymptotic limit of $Nu_{\text{asymp},\hat{L}=4}$ = 29.8, which is lower than that of short plugs ($\hat{L}$= 1). As the plug length increases, the asymptotic limit of *Nu* reduces. This is because of the decrease in the transverse flow, as explained in Fig. 8. The effect of the plug length on the heat transfer index is shown in Fig. 10b. Due to the higher Nusselt numbers in short plugs, the heat transfer process in short plugs is much faster than that in long plugs.

Fig. 11 shows the heat transfer index against plug length at a fixed axial location of the microchannel $\hat{X}$ = 10. The Peclet number is fixed at 100. The temperature distributions of the respective plug length are also shown. The results indicate that as the plug length increases, the heat transfer index decreases. This is because the transverse velocity decreases as $\hat{L}$ increases, which results in a lower *Nu* as shown in Fig. 8 and Fig. 10a. Consequently, long plugs require a longer time and a longer channel length to achieve a uniform temperature T_w.

4. Conclusion

In this paper, the heat transfer of plugs moving in microchannels subjected to a constant-surface-temperature boundary condition is investigated systematically. By incorporating the analytical flow field, the heat transfer process in plugs moving in 2D micro-channels are simulated. The effects of the Peclet number and the plug length are studied. The heat transfer process is evaluated through the Nusselt number, the heat transfer index, and the maximum fluid temperature.

From this study, we can conclude that.

- Heat transfer in plugs can be divided into three stages: (i) development of thermal boundary layer; (ii) advection of heated/ fresh fluid in the plug; and (iii) thermally fully developed flow.
- At a high Peclet number, the Nusselt number experience oscillation when the heated/fresh fluid in the central region of the plug is being transported to the heated wall by the recirculating flow. As the Peclet number decreases, the oscillation of Nusselt number becomes insignificant. A high Peclet number results in a higher Nusselt number and a lower heat transfer index.
- Short plugs are favourable for heat transfer in microchannels as compared to long plugs. In the constant-surface-temperature condition, shorter plugs can achieve higher heat transfer indices due to the higher transverse velocity.

Without numerically solving the flow field and predicting the interface, the method used in this paper to predict and evaluate heat transfer in liquid plug is simple and efficient. It can be used to guide the design of plug-based microchannel heat exchangers, to predict and evaluate heat transfer process within liquid plugs in microchannels, and to deepen our understanding of the effects of the recirculating flow in plugs on the heat and mass transfer process in microchannels.

References

[1] G.L. Morini, Single-phase convective heat transfer in microchannels: a review of experimental results, Int. J. Therm. Sci. 43 (2004) 631–651.

[2] B. Palm, Heat transfer in microchannels, Microsc. Thermophys. Eng. 5 (2001) 155–175.

[3] T.M. Squires, S.R. Quake, Microfluidics: fluid physics at the nanoliter scale, Rev. Modern Phys. 77 (2005) 977–1026.

[4] J. Happel, H. Brenner, Low Reynolds Number Hydrodynamics: With Special Applications to Particulate Media, 2nd ed., Martinus Nijhoff Publishers, The Hague, 1983.

[5] J.M. Ottino, The Kinematics of Mixing: Stretching, Chaos, and Transport, Cambridge University Press, Cambridge, 1989.

[6] W.R. Dean, Note on the motion of fluid in a curved pipe, Philos. Mag. Ser. 7 (4) (1927) 208–223.

[7] S.A. Berger, L. Talbot, L.S. Yao, Flow in curved pipes, Ann. Rev. Fluid Mech. 15 (1983) 461–512.

[8] P. Naphon, S. Wongwises, A review of flow and heat transfer characteristics in curved tubes, Renew. Sustain. Energy Rev. 10 (2006) 463–490.

[9] F. Liu, L. Wang, Analysis on multiplicity and stability of convective heat transfer in tightly curved rectangular ducts, Int. J. Heat Mass Transfer 52 (2009) 5849–5866.

[10] M. Meis, F. Varas, A. Velazquez, J.M. Vega, Heat transfer enhancement in micro-channels caused by vortex promoters, Int. J. Heat Mass Transfer 53 (2010) 29–40.

[11] S. Turki, H. Abbassi, S. Ben Nasrallah, Two-dimensional laminar fluid flow and heat transfer in a channel with a built-in heated square cylinder, Int. J. Therm. Sci. 42 (2003) 1105–1113.

[12] T. Icoz, Y. Jaluria, Design optimization of size and geometry of vortex promoter in a two-dimensional channel, J. Heat Transfer 128 (2006) 1081–1092.

[13] H. Abbassi, S. Turki, S. Ben Nasrallah, Numerical investigation of forced convection in a plane channel with a built-in triangular prism, Int. J. Therm. Sci. 40 (2001) 649–658.

[14] A. Valencia, M. Sen, Unsteady flow and heat transfer in plane channels with spatially periodic vortex generators, Int. J. Heat Mass Transfer 46 (2003) 3189–3199.

[15] A. Kawahara, P.Y. Chung, M. Kawaji, Investigation of two-phase flow pattern, void fraction and pressure drop in a microchannel, Int. J. Multiph. Flow 28 (2002) 1411–1435.

[16] K.A. Triplett, S.M. Ghiaasiaan, S.I. Abdel-Khalik, D.L. Sadowski, Gas-liquid

two-phase flow in microchannels part I: two-phase flow patterns, Int. J. Multiph. Flow 25 (1999) 377–394.
[17] P. Angeli, A. Gavriilidis, Hydrodynamics of Taylor flow in small channels: a review, Proc. Inst. Mech. Eng. C J. Mech. Eng. Sci. 222 (2008) 737–751.
[18] G.F. Christopher, S.L. Anna, Microfluidic methods for generating continuous droplet streams, J. Phys. D Appl. Phys. 40 (2007) R319–R336.
[19] A. Günther, S.A. Khan, M. Thalmann, F. Trachsel, K.F. Jensen, Transport and reaction in microscale segmented gas-liquid flow, Lab on a Chip 4 (2004) 278–286.
[20] K. Handique, M.A. Burns, Mathematical modeling of drop mixing in a slit-type microchannel, J. Micromech. Microeng. 11 (2001) 548–554.
[21] A. Günther, M. Jhunjhunwala, M. Thalmann, M.A. Schmidt, K.F. Jensen, Micromixing of miscible liquids in segmented gas–liquid flow, Langmuir 21 (2005) 1547–1555.
[22] M. Muradoglu, A. Günther, H.A. Stone, A computational study of axial dispersion in segmented gas–liquid flow, Phys. Fluids 19 (2007) 072109.
[23] H. Song, D.L. Chen, R.F. Ismagilov, Reactions in droplets in microfluidic channels, Angewandte Chemie – International Edition 45 (2006) 7336–7356.
[24] J.D. Tice, H. Song, A.D. Lyon, R.F. Ismagilov, Formation of droplets and mixing in multiphase microfluidics at low values of the Reynolds and the capillary numbers, Langmuir 19 (2003) 9127–9133.
[25] Z. Che, N.T. Nguyen, T.N. Wong, Analysis of chaotic mixing in plugs moving in meandering microchannels, Phys. Rev. E 84 (2011) 066309.
[26] E. Baird, K. Mohseni, Digitized heat transfer: a new paradigm for thermal management of compact micro systems, IEEE Trans. Components Packag. Technol. 31 (2008) 143–151.
[27] P.A. Walsh, E.J. Walsh, Y.S. Muzychka, Heat transfer model for gas–liquid slug flows under constant flux, Int. J. Heat Mass Transfer 53 (2010) 3193–3201.
[28] E. Baird, K. Mohseni, Numerical simulations for digitized heat transfer, in: ASME 2009 InterPACK Conference, Vol. 2, pp. 923–931.
[29] X.F. Peng, B.X. Wang, Forced convection and flow boiling heat transfer for liquid flowing through microchannels, Int. J. Heat Mass Transfer 36 (1993) 3421–3427.
[30] J.R. Thome, Boiling in microchannels: a review of experiment and theory, Int. J. Heat Fluid Flow 25 (2004) 128–139.
[31] Y. Chen, P. Cheng, Condensation of steam in silicon microchannels, Int. Commun. Heat Mass Transfer 32 (2005) 175–183.
[32] B.J. Kim, Y.Z. Liu, H.J. Sung, Micro PIV measurement of two-fluid flow with different refractive indices, Measure. Sci. Technol. 15 (2004) 1097–1103.
[33] M. Oishi, H. Kinoshita, T. Fujii, M. Oshima, Confocal micro-PIV measurement of droplet formation in a T-shaped micro-junction,J. Phys. Conf. Ser. 147 (2009)

012061.
[34] Y.S. Muzychka, E. Walsh, P. Walsh, Simple models for laminar thermally developing slug flow in noncircular ducts and channels, J. Heat Transfer 132 (2010) 111702.
[35] R. Scardovelli, S. Zaleski, Direct numerical simulation of free-surface and interfacial flow, Ann. Rev. Fluid Mech. 31 (1999) 567–603.
[36] T. Taha, Z.F. Cui, Hydrodynamics of slug flow inside capillaries, Chem. Eng. Sci. 59 (2004) 1181–1190.
[37] K. Fukagata, N. Kasagi, P. Ua-arayaporn, T. Himeno, Numerical simulation of gas–liquid two-phase flow and convective heat transfer in a micro tube, Int. J. Heat Fluid Flow 28 (2007) 72–82.
[38] S. Osher, R.P. Fedkiw, Level set methods: an overview and some recent results, J. Comput. Phys. 169 (2001) 463–502.
[39] Z. Yu, O. Hemminger, L.-S. Fan, Experiment and lattice boltzmann simulation of two-phase gas-liquid flows in microchannels, Chem. Eng. Sci. 62 (2007) 7172–7183.
[40] J. Zhang, Lattice boltzmann method for microfluidics: models and applications, Microfluid. Nanofluid. 10 (2010) 1–28.
[41] H. Fujioka, J.B. Grotberg, Steady propagation of a liquid plug in a two-dimensional channel, J. Biomech. Eng. Trans. ASME 126 (2004) 567–577.
[42] J. Sivasamy, Z. Che, T.N. Wong, N.-T. Nguyen, L. Yobas, A simple method for evaluating and predicting chaotic advection in microfluidic slugs, Chem. Eng. Sci. 65 (2010) 5382–5391.
[43] S.V. Patankar, Numerical Heat Transfer and Fluid Flow, Series in computational methods in mechanics and thermal sciences, Hemisphere Pub. Corp., Washington, 1980.
[44] F.P. Incropera, D.P. DeWitt, Fundamentals of Heat and Mass Transfer, 5th ed., John Wiley & Sons, New York, 2002.
[45] G. Taylor, Dispersion of soluble matter in solvent flowing slowly through a tube, Proc. Roy. Soc. Lond. Ser. A Math. Phys. Sci. 219 (1953) 186–203.

List of Figures

well.

Fig.9 Recirculating periods for fluid particles in plugs of different lengths. Passive tracer particles along the middle cross section $\hat{x} = \hat{L}/2$ are tracked to find out their recirculating periods for plugs of different lengths.

Fig.10 Nusselt number (a) and heat transfer index (b) in liquid plugs of different lengths. The Peclet number is $Pe = 100$.

Fig.11 Effect of the dimensionless plug length $\hat{L}$ on the heat transfer index η .The axial location of the plug $\hat{X} = 10$, and the Peclet number is $Pe = 100$. The temperature distribution within the plugs are shown.

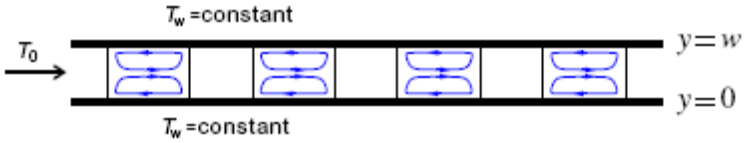

Fig.1

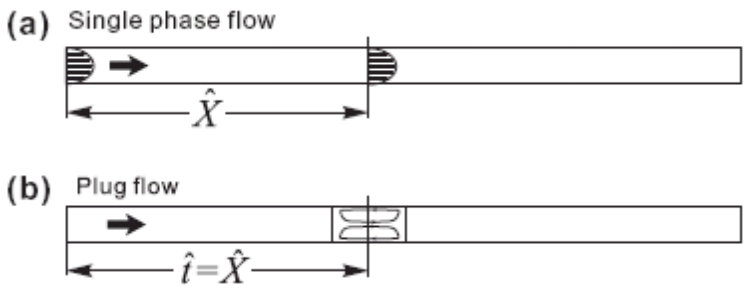

Fig.2

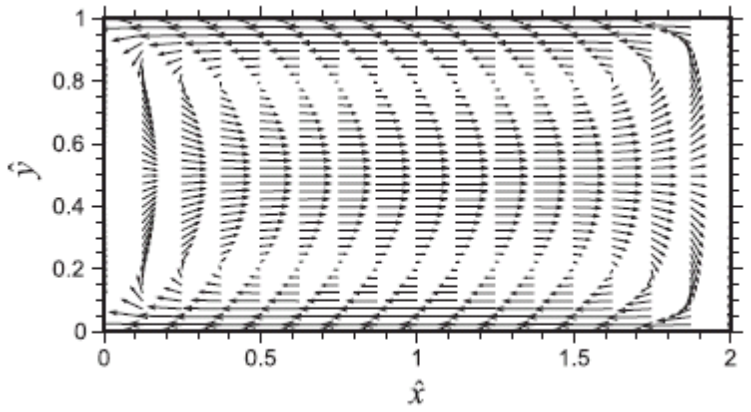

Fig.3

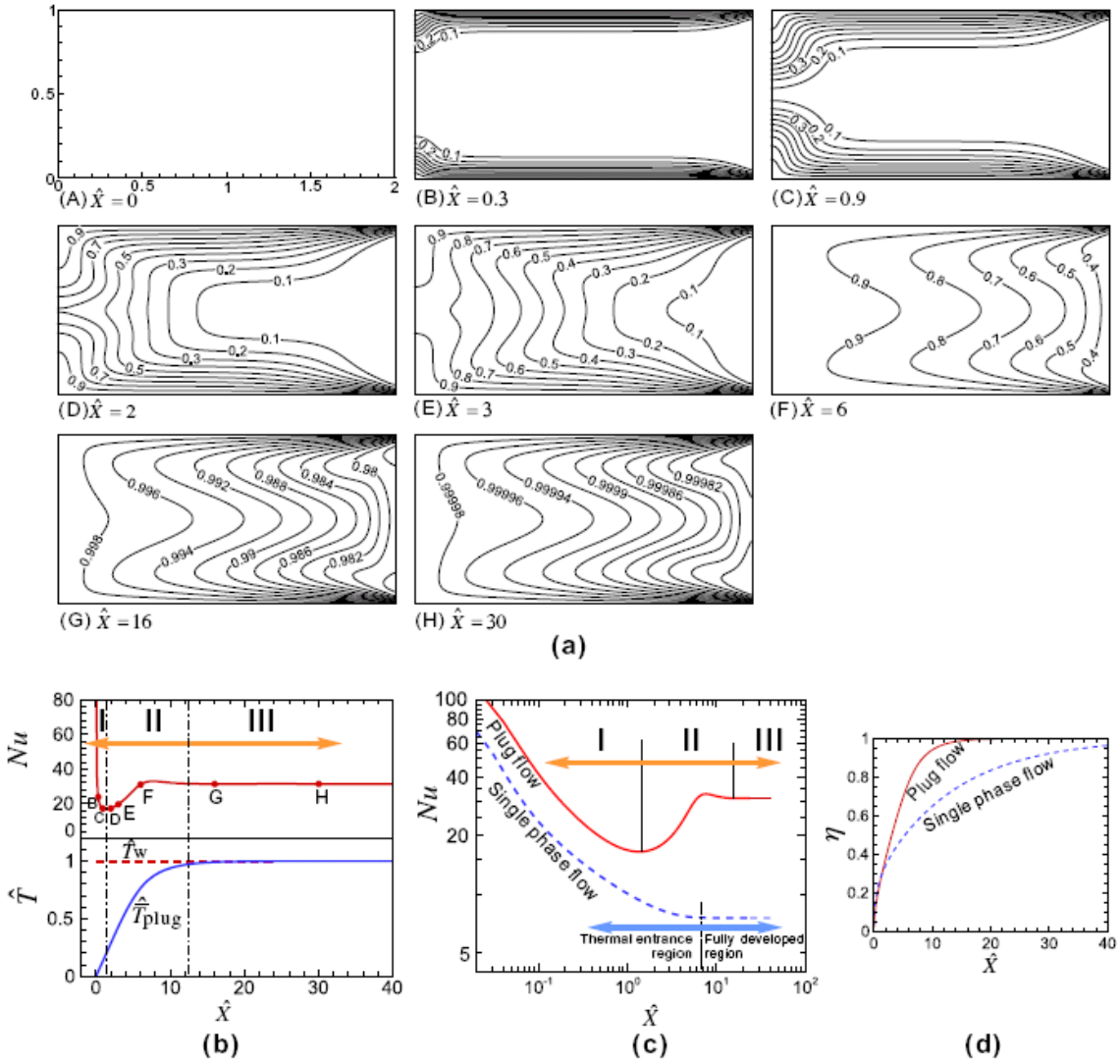
(A) $\hat{X}=0$
(B) $\hat{X}=0.3$
(C) $\hat{X}=0.9$
(D) $\hat{X}=2$
(E) $\hat{X}=3$
(F) $\hat{X}=6$
(G) $\hat{X}=16$
(H) $\hat{X}=30$
(a)
I
II
III
B
C
D
E
F
G
H
$\hat{T}_w$
$\hat{\bar{T}}_{plug}$
Nu
$\hat{T}$
$\hat{X}$
(b)
Plug flow
Single phase flow
Thermal entrance region
Fully developed region
(c)
η
(d)

Fig.4

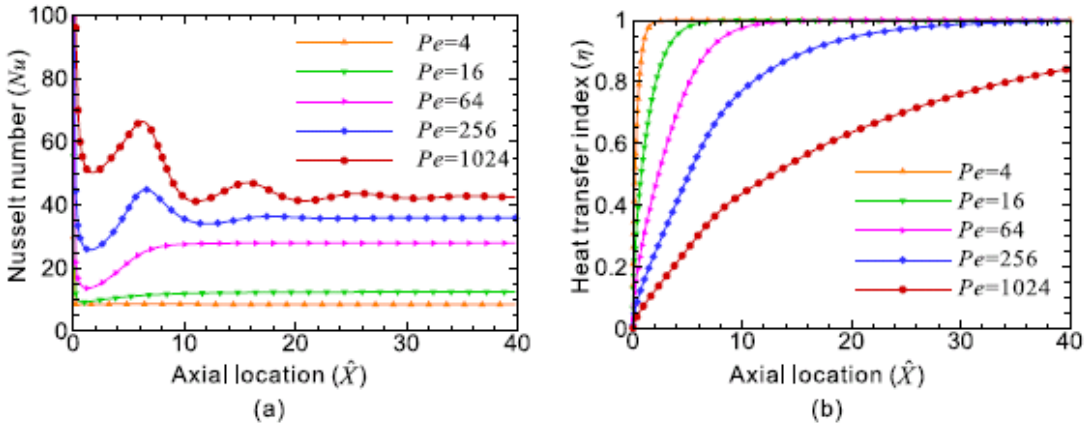
Nusselt number (Nu)
Axial location ($\hat{X}$)
(a)
Pe=4
Pe=16
Pe=64
Pe=256
Pe=1024
Heat transfer index (η)
Axial location ($\hat{X}$)
(b)
Pe=4
Pe=16
Pe=64
Pe=256
Pe=1024

Fig.5

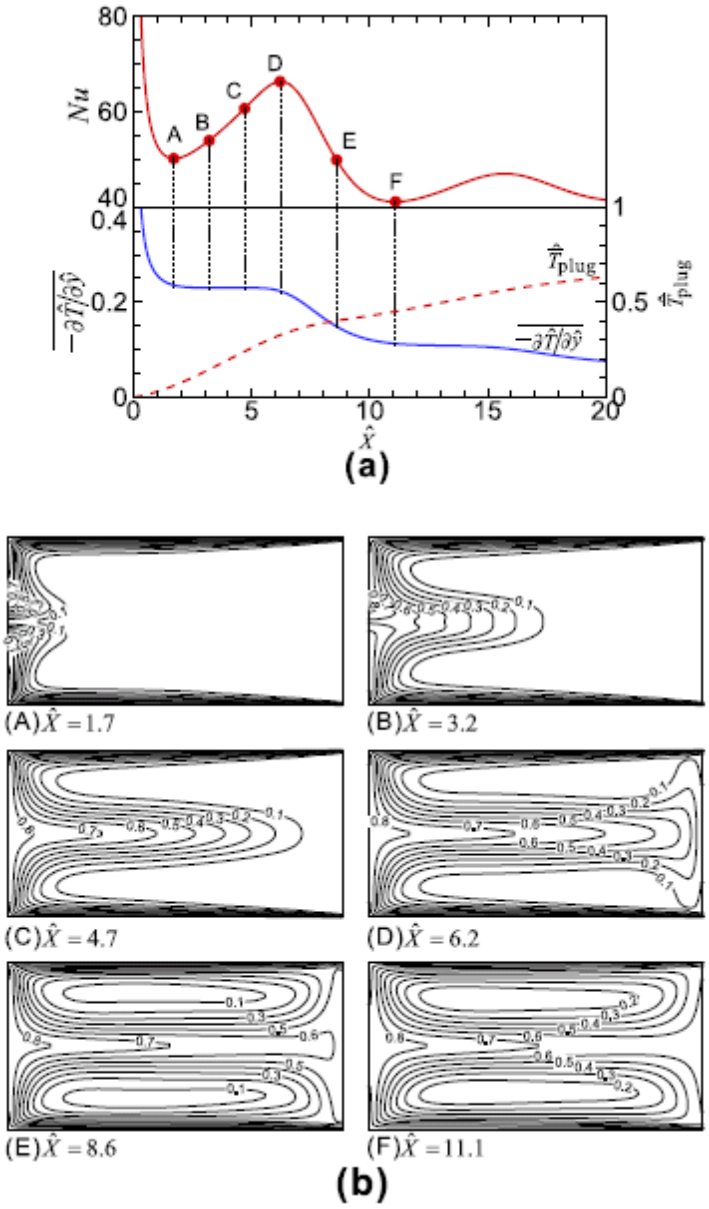
80
60
40
Nu
A
B
C
D
E
F
0.4
0.2
0
0
5
10
15
20
1
0.5
0
$\hat{X}$
$\overline{\hat{T}}_{plug}$
$-\overline{\partial \hat{T}/\partial \hat{y}}$
(a)
(A) $\hat{X}=1.7$
(B) $\hat{X}=3.2$
(C) $\hat{X}=4.7$
(D) $\hat{X}=6.2$
(E) $\hat{X}=8.6$
(F) $\hat{X}=11.1$
(b)

Fig.6

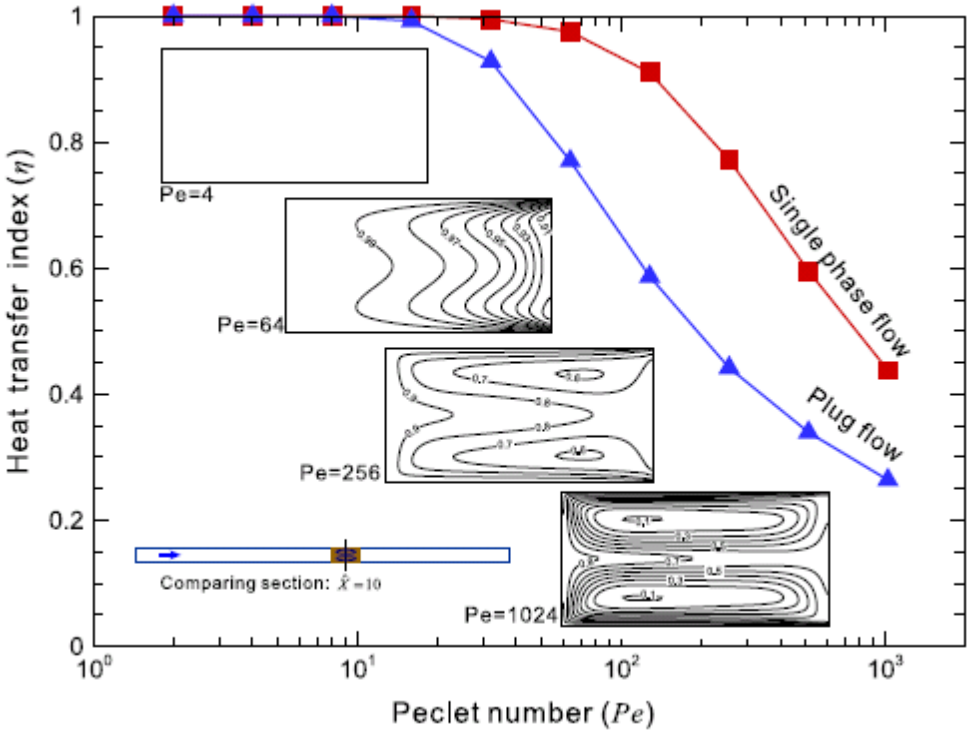
Heat transfer index (η)
Peclet number (Pe)
Single phase flow
Plug flow
Pe=4
Pe=64
Pe=256
Pe=1024
Comparing section: $\hat{X}=10$

Fig.7

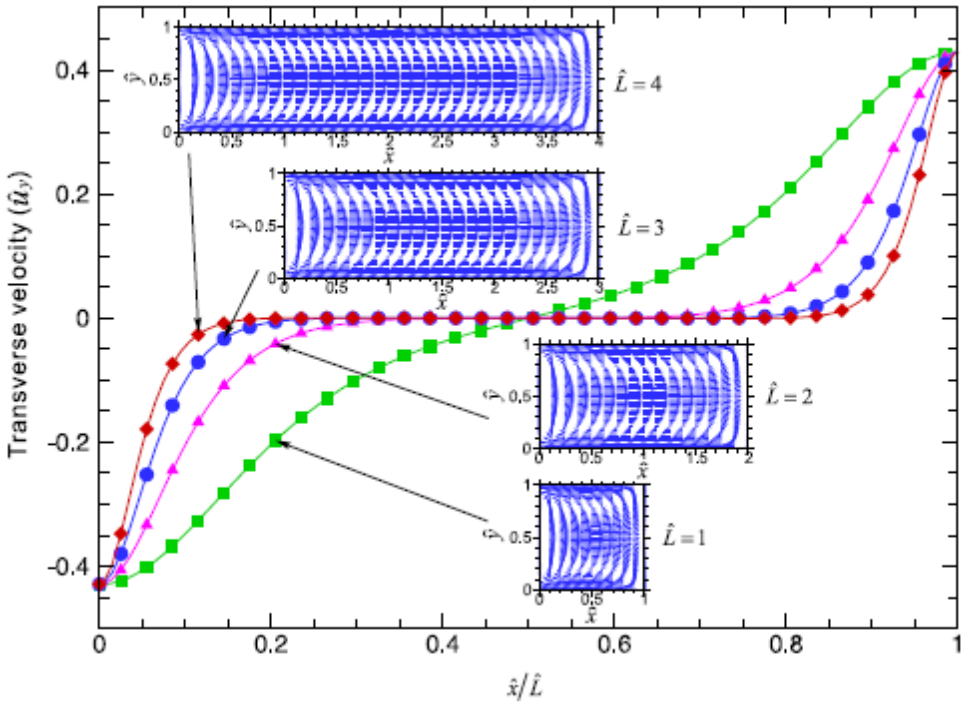
Transverse velocity ($\hat{u}_y$)
$\hat{x}/\hat{L}$
$\hat{L}=4$
$\hat{L}=3$
$\hat{L}=2$
$\hat{L}=1$

Fig.8

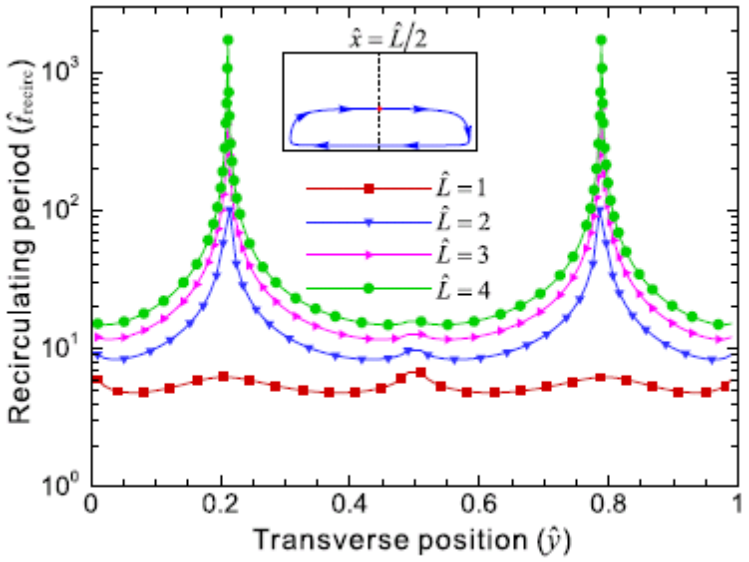
$\hat{x} = \hat{L}/2$
$\hat{L} = 1$
$\hat{L} = 2$
$\hat{L} = 3$
$\hat{L} = 4$
Recirculating period ($\hat{t}_{receire}$)
Transverse position ($\hat{y}$)
10^0
10^1
10^2
10^3
0
0.2
0.4
0.6
0.8
1

Fig.9

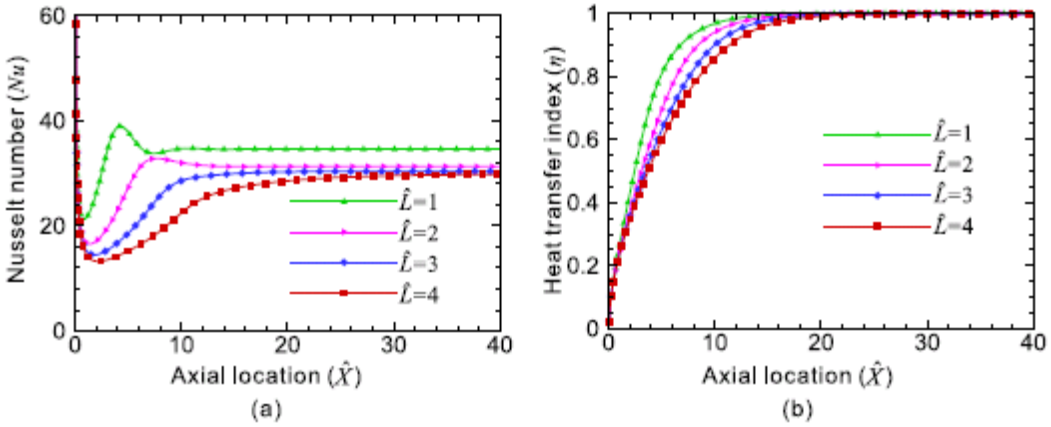
Nusselt number (Nu)
Axial location ($\hat{X}$)
(a)
Heat transfer index (η)
Axial location ($\hat{X}$)
(b)
$\hat{L}$=1
$\hat{L}$=2
$\hat{L}$=3
$\hat{L}$=4

Fig.10

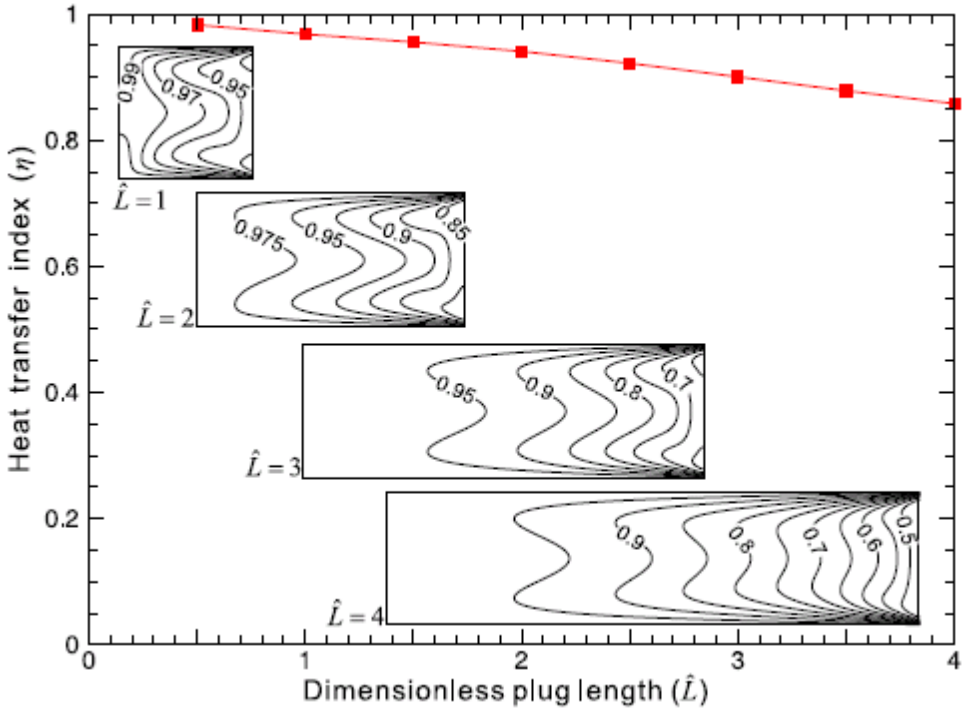
Heat transfer index (η)
Dimensionless plug length ($\hat{L}$)
0
0.2
0.4
0.6
0.8
1
0
1
2
3
4
$\hat{L}=1$
0.99
0.97
0.95
$\hat{L}=2$
0.975
0.95
0.9
0.85
$\hat{L}=3$
0.95
0.9
0.8
0.7
$\hat{L}=4$
0.9
0.8
0.7
0.6
0.5

Fig.11